



# Human ribosomal G-quadruplexes regulate heme bioavailability

Received for publication, May 12, 2020, and in revised form, August 6, 2020. Published, Papers in Press, August 13, 2020. DOI 10.1074/jbc.RA120.014332

Santi Mestre-Fos<sup>1,2,3</sup> , Chieri Ito<sup>1,2,3</sup>, Courtney M. Moore<sup>2,3</sup> , Amit R. Reddi<sup>2,3,4,\*</sup>, and Loren Dean Williams<sup>1,2,3,4,\*</sup>

From the <sup>1</sup>Center for the Origin of Life, <sup>2</sup>School of Chemistry and Biochemistry, <sup>3</sup>Parker Petit Institute of Bioengineering and Biosciences, and <sup>4</sup>School of Biological Sciences, Georgia Institute of Technology, Atlanta, Georgia, USA

Edited by Karin Musier-Forsyth

The *in vitro* formation of stable G-quadruplexes (G4s) in human rRNA was recently reported. However, their formation in cells and their cellular roles were not resolved. Here, by taking a chemical biology approach that integrates results from immunofluorescence, G4 ligands, heme-affinity reagents, and a genetically encoded fluorescent heme sensor, we report that human ribosomes can form G4s *in vivo* that regulate heme bioavailability. Immunofluorescence experiments indicate that the vast majority of extra-nuclear G4s are associated with rRNA. Moreover, titrating human cells with a G4 ligand alters the ability of ribosomes to bind heme and disrupts cellular heme bioavailability as measured by a genetically encoded fluorescent heme sensor. Overall, these results suggest that ribosomes play a role in regulating heme homeostasis.

Heme (iron protoporphyrin IX) is an essential but potentially cytotoxic metallocofactor and signaling molecule required for much of life on Earth. All heme-requiring cells and organisms must tightly regulate heme concentration and bioavailability to mitigate toxicity (1–4). Proteins that synthesize and degrade heme are relatively well-understood; structures and mechanisms of all eight heme biosynthetic enzymes and heme-degrading heme oxygenases are known (2–4). However, regulation of heme bioavailability, including its intracellular trafficking from sites of synthesis in the mitochondrial matrix or uptake at the plasma membrane, is poorly understood. Current paradigms for heme trafficking and mobilization involve heme transfer by unknown proteinaceous factors and largely ignore contributions from nucleic acids. Given that the first opportunity for protein hemylation occurs during or just after translation, rRNA or ribosomal proteins (rProteins) may be critical for shepherding labile heme to newly synthesized proteins.

We hypothesize that heme bioavailability is regulated in part by ribosomes via rRNA G-tracts, which are continuous runs of guanines. G-tracts are confined primarily to ribosomes of birds and mammals (5) and are focused in rRNA tentacles, which are seen to extend for hundreds of Å from ribosomal surfaces in these species (6). Tentacles are elaborations of rRNA expansion segments, which help form the secondary shell around the common core of eukaryotic ribosomes (7).

Tandem G-tracts can form G-quadruplexes (G4s), which are nucleic acid secondary structures composed of four guanine columns surrounding a central cavity that sequesters monovalent cations. Our rRNA<sup>G4</sup>-heme hypothesis is based in part on our observation of stable rRNA G4s *in vitro* (5, 8) and the extraordinary abundance of rRNA *in vivo* (9). Our rRNA<sup>G4</sup>-heme hypothesis is also based on work by Sen and co-workers (10–12), who has demonstrated high affinity of heme for G4s ( $K_D \sim \text{nM}$ ) and proposed that RNA and DNA G4s sequester heme *in vivo* (13).

DNA G4s are thought to help regulate replication (14), transcription (15), and genomic stability (16). In mRNA, G4s are associated with untranslated regions and have been proposed to regulate translation (17–19). However, the *in vivo* folding state and functional roles of G4s are under debate. It has been proposed that eukaryotic RNA G4s are unfolded by helicases (20), although some investigators are not convinced (21, 22). The density of G4 sequences on surfaces of the human ribosome, which is extremely abundant, is high, with 17 G4 sequences in the 28S rRNA and three in 18S rRNA (Fig. 1A). Previous to this report, it was not known whether human ribosomes form G4s *in vivo* or what their functions might be.

Here we present evidence that human rRNA tentacles form G4s *in vivo* that regulate cellular heme homeostasis. Results of immunofluorescence experiments with a G4 antibody, RNA pulldowns, and experiments with well-characterized G4 ligands provide strong support for *in vivo* formation of surface-exposed G4s on rRNA tentacles. We find that G4s on ribosomes bind heme *in vitro* (Fig. 1B) and that perturbation of G4s *in vivo* with G4 ligands affects heme interactions and bioavailability, as measured by heme-affinity reagents and genetically encoded heme sensors. The effects of *in vivo* G4-heme perturbations are predicted by *in vitro* experiments. Taken together, the results here indicate that rRNA G4s interact with heme in cells and suggest that ribosomal G4s play roles in intracellular heme metabolism.

## Results

### rRNA forms G4s *in vivo*

Confocal microscopy and G4-pulldowns were used to determine whether human ribosomes form G4s *in vivo*. For confocal microscopy, we used the BG4 antibody, which selectively targets G4s (23, 24) and has been broadly used for visualizing DNA G4s and non-rRNA G4s in cells (24–27). Our method of permeabilizing cells for antibody treatment does not permeabilize the nuclei (28). Therefore, DNA G4s were not anticipated or observed. To

This article contains supporting information.

\*For correspondence: Loren Dean Williams, [loren.williams@chemistry.gatech.edu](mailto:loren.williams@chemistry.gatech.edu); Amit R. Reddi, [amit.reddi@chemistry.gatech.edu](mailto:amit.reddi@chemistry.gatech.edu).

## Human ribosomes appropriate heme

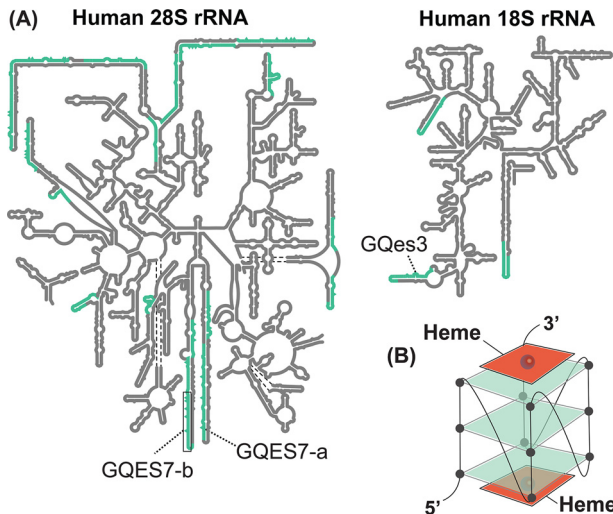


**Figure 1.** A, secondary structures of the human LSU rRNAs (5.8S and 28S) and SSU rRNA (18S). G4 sequences are highlighted in green. rRNA-based oligomers from the LSU (GQES7-a and GQES7-b) and from the SSU (GQes3) are indicated. B, schematic representation of a heme-G4 complex.

identify ribosome-associated G4s, we determined the extent to which antibodies to rProtein L19 (eL19) and to G4s colocalize and how colocalization is altered when cells are subjected to RNase or G4 ligand PhenDC3. Prior to antibody addition, the cells were cross-linked with paraformaldehyde, which has been shown to lock G4s *in situ* and reduce induction of G4s by small ligands (22). The extent of L19 and G4 antibody colocalization suggests that a fraction of ribosomes form G4s (Fig. 2, A and C) and that most G4s are associated with ribosomes. Specifically, we find that ~83% of BG4 colocalizes with L19, indicating that the vast majority of RNA G4s *in vivo* are associated with ribosomes (Fig. 2C, green bar) and are therefore rRNA G4s. Conversely, only 5% of L19 colocalizes with BG4 (Fig. 2C, WT red bar), indicating that only a specialized fraction of ribosomes contain G4s. Similar results were obtained using an antibody against rProtein uL4 instead of eL19 (not shown). It is possible that the polymorphic nature of rRNA G4s attenuates binding to BG4, contributing to low colocalization ratios.

PhenDC3 (3,3'-[1,10-phenanthroline-2,9-diylbis(carboxylimino)]bis[1-methyl quinolinium] 1,1,1-trifluoromethanesulfonate) is a bisquinolinium phenanthroline derivative known to induce and stabilize G4s (29–32). Here, PhenDC3 appears to increase ribosomal G4 formation *in vivo*; treating cells with PhenDC3 increases L19-BG4 colocalization from 5 to ~24% (Fig. 2C). The increase in colocalization upon PhenDC3 treatment supports formation of G4s by ribosomes. By contrast, treating cells with RNase A abolishes the L19-BG4 colocalization signal (Fig. 2C). Together, these results indicate that the colocalized BG4 signal is from a G4-forming RNA in close proximity to L19.

The high density of ribosomes on the surface of the endoplasmic reticulum (ER) and the lower abundance of mRNA in this location as compared with the cytosol (33) motivated us to investigate whether G4s colocalize with the ER. mRNAs in the cytosol, in the unlikely event that they form G4s at high frequency (20), may confound our ability to selectively detect rRNA G4s. Toward this end, we determined the extent to which BG4 colocalizes with an antibody against an ER mem-

brane protein (calnexin) (Fig. 2B). Indeed, we find that ~45% of the BG4 signal colocalizes with the ER surface (Fig. 2D, green bar), indicating a significant presence of RNA G4s near the ER membrane. As with L19, the fraction of the ER signal that colocalizes with G4s is completely abolished by RNase A and enhanced by PhenDC3 (increasing from 2 to 12%) (Fig. 2D). Thus, the data are consistent with formation of rRNA G4s by ER-bound ribosomes.

In an orthogonal approach, we pulled down RNA with BioTASQ (22, 34), a G4 ligand linked to biotin that captures G4s. We previously used BioTASQ to demonstrate that human rRNA forms G4s *in vitro* (Fig. 2E) (8). Here, we captured rRNA G4s from cross-linked HEK293 cells by methods summarized in Fig. 2F. BioTASQ captures 28S rRNA from cell lysates (Fig. 2G), in agreement with our previous *in vitro* BioTASQ data and with observations of G4-L19 colocalization above. BioTASQ also captures 18S rRNA, although the signal is significantly weaker. This observation is in agreement with the greater abundance of G-tracts in human 28S rRNA (17 G4 regions) than in 18S rRNA (three G4 regions). Taken together, our immunofluorescence and BioTASQ experiments provide strong evidence that human ribosomes form G4s *in vivo*.

### Human ribosomes bind hemin *in vitro*

It has been suggested that G4s might associate with heme *in vivo* (10, 11, 35). *In vitro*, heme binds with high affinity to G4s by end-stacking (10–12, 36–38) (Fig. 1B). Here, we used UV-visible spectroscopy to assay the binding of hemin to human rRNA. rRNA oligomers GQES7-a (Fig. 3A), GQES7-b (Fig. S1A), or GQes3 (Fig. S1B) were titrated into fixed amount of hemin. GQES7-a and GQES7-b are fragments of expansion segment 7 of human large subunit (LSU) rRNA (5). GQes3 is a fragment of expansion segment 3 of human small subunit (SSU) rRNA (8). Each of these oligonucleotides is known to form G4s, and each caused a pronounced increase in the Soret band of hemin at 400 nm. The binding is specific for G4s because a mutant oligonucleotide, *mutes3*, that lacks G-tracts does not induce a change in the hemin Soret band (Fig. S1C). Larger human ribosomal components also bind heme. Intact 28S and 18S rRNAs extracted from human cells (Fig. S1, D and E), assembled LSUs (Fig. 3B) and SSUs (Fig. S1F), and polyosomes (Fig. 3C) all induce changes in the hemin Soret bands, which is indicative of heme-rRNA interactions. Fitting of the UV-visible data in Fig. 3A, using a one-site binding model yielded an apparent limiting  $K_D$  value of <100 nM (Fig. 3H), which is similar to that of other G4s (10–12, 39). The combined data are consistent with a model in which rRNA tentacles of human ribosomes bind to hemin *in vitro*.

PhenDC3 was used to confirm binding of hemin to ribosomal G4s under initial conditions that favor G4 formation. PhenDC3, like hemin, end-stacks on G4s (30, 35). *In vitro*, under conditions favoring G4s (50 mM  $K^+$ ), essentially all rRNA G-tracts form stable G4s prior to PhenDC3 addition (5, 8). Under these conditions, PhenDC3 competed with heme for binding to rRNA G4s (Fig. 3, D–F). With fixed concentrations of GQES7-a and hemin, addition of PhenDC3 decreased the intensity of the hemin Soret peak (Fig. 3D) because of dissociation

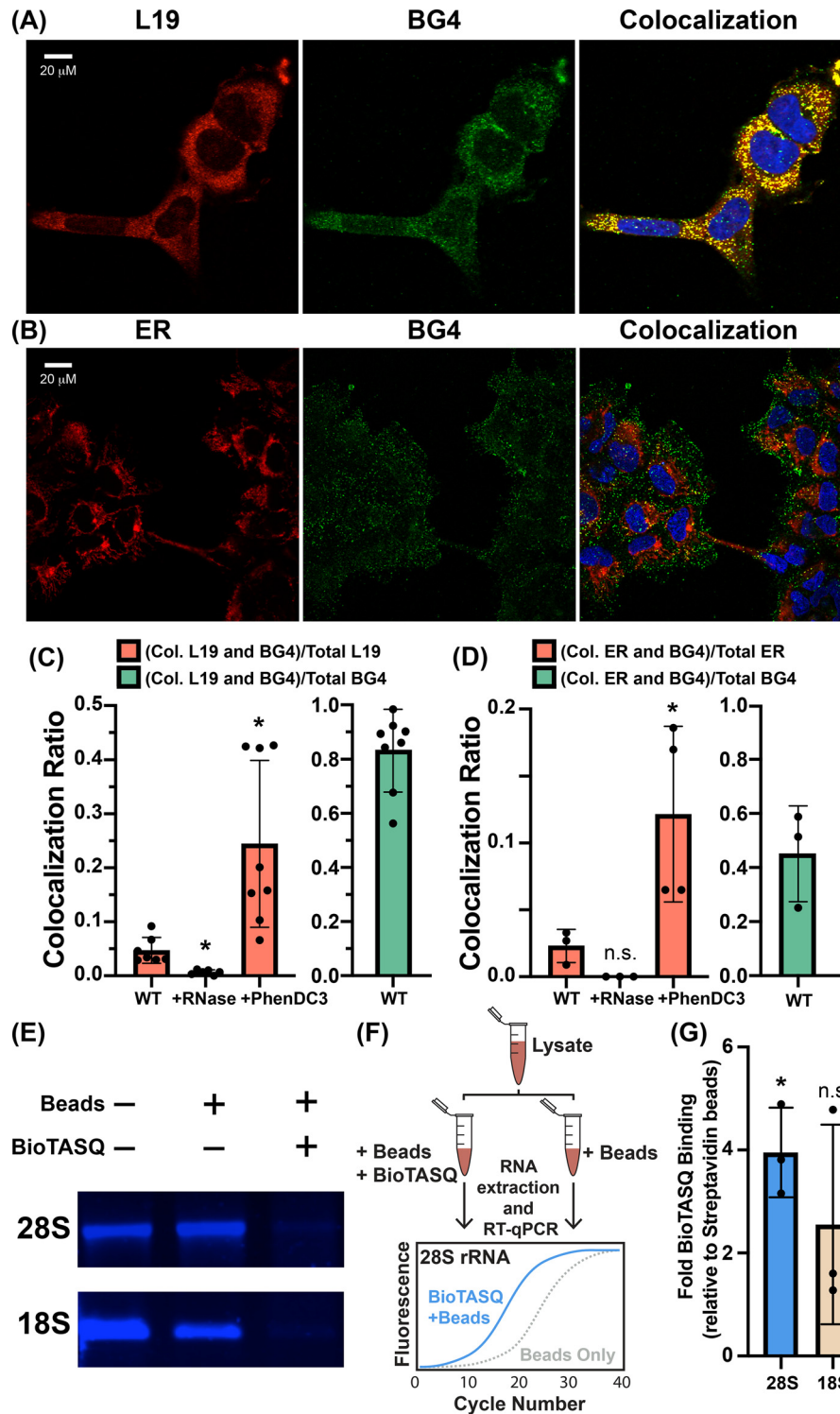


**Figure 2. rRNA G4s in HEK293 cells.** Colocalization of (A) ribosomal protein L19 or (B) endoplasmic reticulum (red) with RNA G4s (green). Nuclei were stained with 4',6-diamidino-2-phenylindole (blue). C, extent of colocalization is quantitated as the ratio of colocalized pixels over total L19 pixels (red bars) or as the ratio of colocalized pixels over total BG4 pixels (green bar). The same analysis was performed for ER-BG4 colocalization (D). The statistical significance relative to WT is indicated by asterisks using an ordinary one-way analysis of variance with Dunnett's post-hoc test. Each dot represents a biological replicate. Images of cells treated without primary antibodies or with RNase A or PhenDC3 are shown in Fig. S6 and Fig. S7. E, the G4 ligand BioTASQ binds to 28S and 18S rRNAs *in vitro*. In the presence of BioTASQ and streptavidin beads, human rRNAs do not enter the native agarose gel. F, schematic representation of the BioTASQ pull-down protocol. G, RT-qPCR analysis of rRNAs pulled down by BioTASQ. The statistical significance relative to a fold-enrichment value of 1 is indicated by asterisks using a one-sample *t* test and a Wilcoxon test. Each dot represents a biological replicate. Data in (G) are represented as RNA enrichment under BioTASQ + streptavidin beads conditions relative to control streptavidin beads. \**p* < 0.05. *n.s.*, not significant.

## Human ribosomes appropriate heme

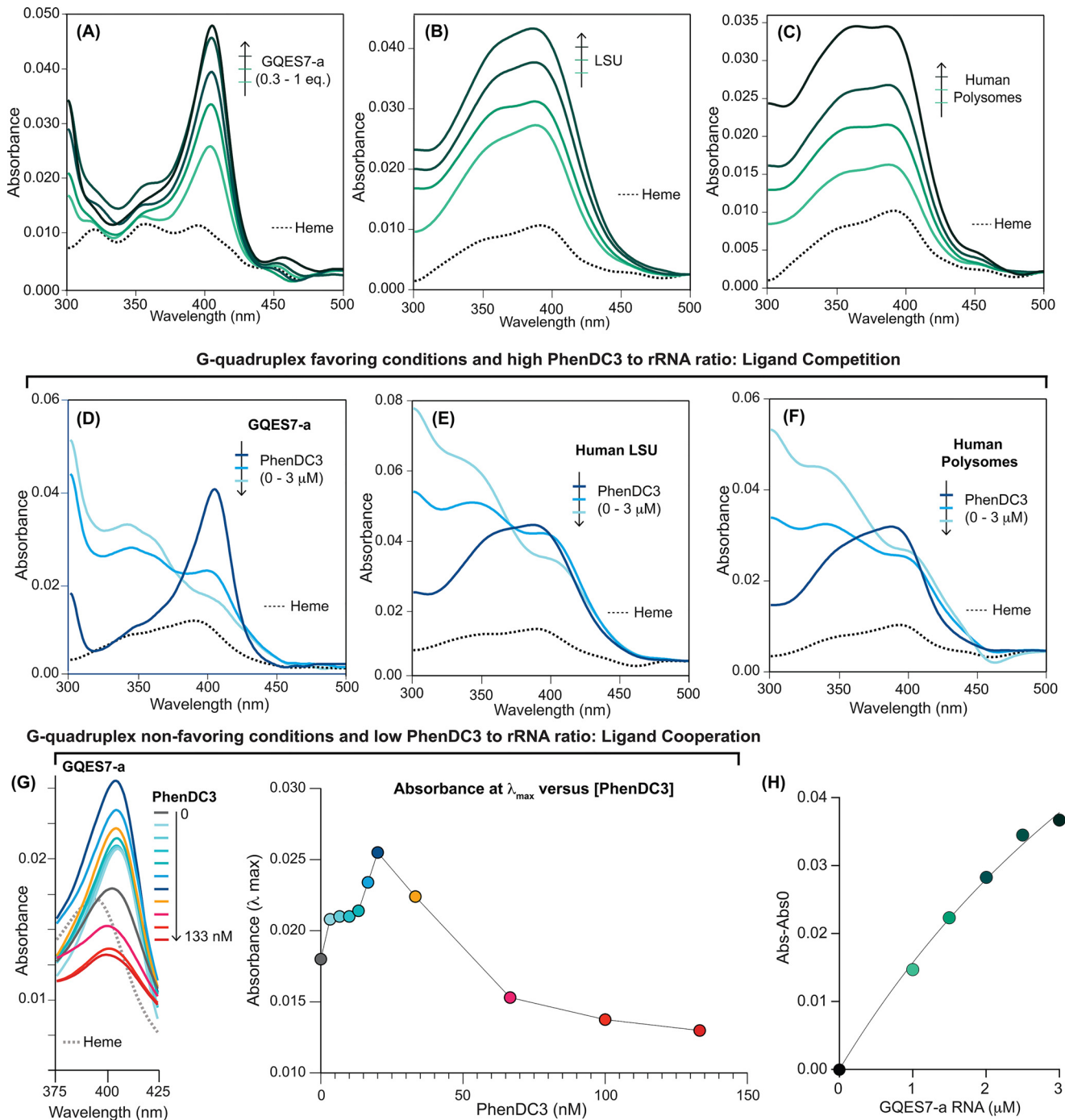


**Figure 3. Human rRNA G4s bind to heme *in vitro*.** UV-visible spectra (the heme Soret band) during heme titration under initial conditions that favor G4 formation with (A) GQES7-a, (B) the assembled LSU, or (C) polysomes. UV-visible spectra during titration with PhenDC3 of (D) constant [heme] and [GQES7-a], (E) constant [heme] and [LSU], and (F) constant [heme] and [polysomes]. G, UV-visible spectra during titration of constant [heme] and [GQES7-a] under initial conditions that favor G4 unfolding. The absorbance at  $\lambda_{\max}$  versus [PhenDC3] is plotted on the panel on the right. H, plot of absorbance at 400 nm versus [GQES7-a]. Data in (A) were fit to a one-site binding model (black line) giving an apparent limiting  $K_D$  of  $<100$  nM. The experiments in panels D–F were performed using initial conditions that favored G4 formation by G-tracts (50 mM  $K^+$  with titration of PhenDC3 in the  $\mu$ M range). The experiment in panel G was performed using initial conditions that favored unfolded G-tracts (10 mM  $Li^+$ , 0  $K^+$  with titration of PhenDC3 nM range).

of heme. The same phenomenon was observed with assembled ribosomal particles (LSU: Fig. 3E, SSU: Fig. S2A) and with polysomes (Fig. 3F). Hemin associated with purified 28S and 18S rRNAs is dissociated by addition of PhenDC3 (Fig. S2, B and C). Solutions of hemin with control RNA *mut3* do not show a change in the Soret peak intensity upon the addition of PhenDC3 (Fig. S2D). PhenDC3 absorbs at 350 nm (Fig. S2E),

causing a shoulder on the heme Soret band (Fig. 3, D–F). The results here provide strong support for association of heme with G4s of human ribosomes *in vitro*.

Unlike the *in vitro* experiments with  $K^+$ , it seems probable that most rRNA G-tracts are unfolded in cells. This inference is based on our observation that only 5% of ribosomes bind to the BG4 antibody *in vivo* until the addition of PhenDC3, upon

which BG4 binding increases to 24% of ribosomes (Fig. 2, C and D). This inefficient folding of G-tracts into G4s in our *in vivo* experiments is in agreement with previous studies (20).

We mimicked the *in vivo* environment using initial conditions that favor unfolded G4s ( $\text{Li}^+$ , low PhenDC3) by GQES7-a rRNA. Under these conditions, we observed that PhenDC3 caused an *increase* in the binding of heme to rRNA G4s at concentrations below 25 nM PhenDC3, as inferred from an increase in the absorbance of the heme Soret peak (Fig. 3G). However, at PhenDC3 concentrations above 25 nM, we observed a *decrease* in the binding of heme to rRNA G4s, as indicated by a reduction in the absorbance of the heme Soret band (Fig. 3G). Thus, under initial conditions that favor unfolded G-tracts ( $\text{Li}^+$ ), low PhenDC3 enhanced heme-binding to GQES7-a. The cooperative relationship between PhenDC3 and heme under some conditions is expected because multiple ligand binding sites are formed by a single binding event (30). On the other hand, under initial conditions that favor folding of G-tracts to G4s ( $\text{K}^+$ ), PhenDC3 acted as a competitor of heme-binding to GQES7-a. It seems possible that formation of G4s by the extended arrays of G-tracts in rRNAs might be cooperative, although to our knowledge this has not been demonstrated.

#### Human ribosomes bind heme *in vivo*

We developed an assay that exploits differential interactions with hemin-agarose, an agarose resin covalently linked to heme, to report *in vivo* heme-binding to ribosomes and rRNA. The degree to which any biomolecule interacts with heme in cells is inversely correlated with the extent to which it interacts with hemin-agarose upon lysis because of competition between endogenous heme and hemin-agarose. Therefore, the effects of heme-binding factors *in vivo* can be monitored by determining whether their interaction with hemin-agarose changes upon depletion of intracellular heme.

Accordingly, HEK293 cells were grown with or without succinylacetone (SA) (40), an inhibitor of heme biosynthesis. Lysates of these cells were incubated with hemin-agarose, and hemin-agarose-interacting rRNA was quantified by RT-qPCR. Consistent with previous work (41), treatment with 0.5 mM SA for 24 h caused a 7-fold decrease in total cellular heme in HEK293 cells (results not shown). The results reveal that rRNA binding to hemin-agarose relative to control agarose lacking heme increases by ~4-fold in cells depleted of heme (Fig. 4A). This result suggests that under heme-depleted conditions, a greater fraction of rRNA-heme-binding sites are free and available to bind hemin-agarose. In short, the data are consistent with a model in which ribosomal RNAs associate with endogenous heme.

#### PhenDC3 treatment of cells increases binding of ribosomes to hemin-agarose

To probe rRNA<sup>G4</sup>-heme-binding *in vivo*, we determined whether rRNA from HEK293 cells treated with the G4 ligand PhenDC3 (48 h at 37 °C) would bind more extensively to hemin-agarose. RT-qPCR reveals that PhenDC3 treatment of HEK293 cells causes a dose-dependent increase in binding of the LSU to hemin-agarose (Fig. 4B). A corresponding but

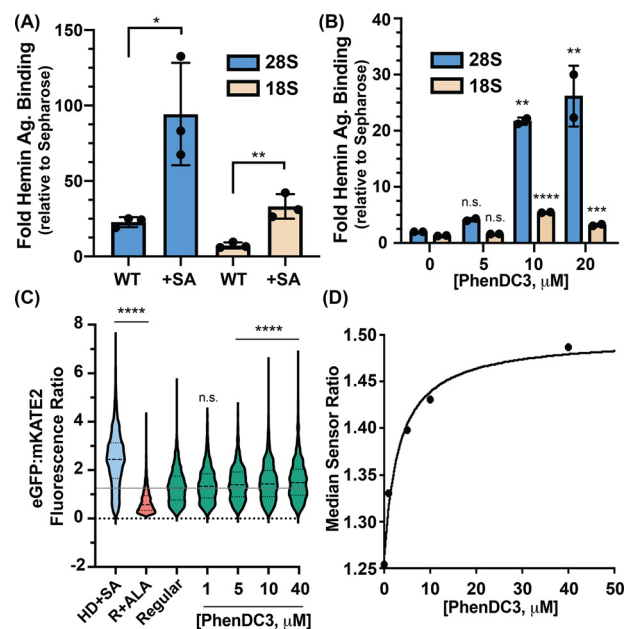


**Figure 4. Ribosomes appropriate heme *in vivo* through rRNA G4s.** A, RT-qPCR analysis from untreated (WT) and SA-treated human cells. Statistical significance relative to WT is represented by asterisks using Student's *t* test. Each dot represents a biological replicate. B, RT-qPCR analysis from PhenDC3-treated HEK293 cells. Statistical significance relative to no-treatment conditions is represented by asterisks using ordinary one-way analysis of variance with Dunnett's post-hoc test. Each dot represents a technical replicate coming from individual biological replicates. The experiment was performed two times with similar dose-dependent trends (Fig. S3A). Data in (A) and (B) are represented as RNA enrichment in hemin-agarose beads relative to control Sepharse beads. C, single-cell analysis of HS1-transfected HEK293 cells grown in HD+SA, regular media containing 5-aminolevulinic acid (R+ALA), or regular media (regular) with the indicated concentrations of PhenDC3. Statistical significance relative to regular conditions is represented by asterisks using the Kruskal-Wallis analysis of variance with Dunn's post-hoc test. \**p* < 0.05, \*\**p* < 0.01, \*\*\**p* < 0.001, \*\*\*\**p* < 0.0001; n.s., not significant; *n* ≥ 1500 cells. D, median HS1 sensor ratios obtained in (C) as a function to PhenDC3 concentration.

weaker signal is seen for the SSU, in agreement with the higher abundance of G4 regions in the LSU than in the SSU (Fig. 1A). These data are consistent with our observations that PhenDC3 promotes rRNA G4 formation in cells (Fig. 2, C–D), providing additional heme-binding sites that can interact with hemin-agarose. Control experiments show that PhenDC3 as used here does not alter rRNA levels (Fig. S4) and that carrier DMSO does not affect the results (Fig. S3, B and C).

#### rRNA G4s regulate heme bioavailability *in vivo*

To determine whether rRNA G4s regulate heme homeostasis, we deployed a previously described genetically encoded ratiometric fluorescent heme sensor, HS1. HS1 is a tri-domain fusion protein consisting of heme-binding domain cytochrome *b*<sub>562</sub> fused to two fluorescent proteins. The fluorescence of eGFP is quenched by heme, and the fluorescence of mKate2 is unaltered by heme. Thus, the ratio of eGFP:mKate2 fluorescence is inversely correlated with bioavailable heme, as measured by HS1. HS1 was previously used to characterize heme homeostasis in yeast, bacteria, and mammalian cells and was instrumental in identifying new heme-trafficking factors and signals that alter heme biodistribution and dynamics (40, 42–44). We asked if cytosolic heme bioavailability is altered in

## Human ribosomes appropriate heme

response to G4 ligand PhenDC3 (40). As indicated in Fig. 4C, single-cell analysis of a population of ~1500 HEK293 cells/condition indicated that the median HS1 eGFP/mKate2 ratio increased upon heme depletion in heme-deficient media containing SA (HD+SA) and decreased upon increasing intracellular heme when cells were conditioned with the heme biosynthetic precursor 5-aminolevulinic acid (ALA) to drive heme synthesis. Upon exposure to PhenDC3 for 24 h, which is the minimal amount of time needed to observe an effect on labile heme (Fig. S5), the HS1 sensor ratio increased in response to increasing PhenDC3 dose, indicating a decrease in heme bioavailability. This 24-h treatment is similar to treatment times used previously for small-molecule induction of G4s in cells (23, 24, 35). The difference in the time required for PhenDC3 to affect heme *in vivo* (24 h) versus *in vitro* (15 min) is likely due to the kinetics of PhenDC3 cellular import, its partitioning into rRNA, and its induction of G4 formation, followed by the consequent reequilibration of cellular heme into G4 heme-binding sites. Regardless, these observations are in agreement with our data in Fig. 3G. PhenDC3 induced G4 formation *in vivo*, increasing the heme-binding sites on the rRNA that can bind heme. Consequently, there was a decrease in the bioavailable heme as detected by HS1. The fractional heme saturation of HS1 decreased by ~15% (Fig. 4D), which is on the order of what one would expect based on an equilibrium competition model between HS1 and intracellular rRNA G4s that takes into account the relative abundance of these species and their Fe(III)-heme affinities (Fig. S8). Our data indicate that rRNA G4s bind heme and regulate intracellular heme bioavailability.

## Discussion

Over the last two decades, whereas a handful of proteins have been implicated in regulating heme homeostasis on the basis of binding heme *in vitro*, there has been very little evidence of such roles from in-cell or *in vivo* studies (2–4, 45). Two notable exceptions include GAPDH and progesterone receptor membrane component 1 and 2. GAPDH, a key glycolytic enzyme, was found to bind and buffer heme, regulating its bioavailability (40, 43), and to deliver heme to nuclear heme-dependent transcription factors (40) and heme enzymes such as nitric oxide synthase (43, 46) and guanylate cyclase (47). Progesterone receptor membrane components, which interact with the terminal heme synthetic enzyme, ferrochelatase (48), have long been known to bind heme and affect the activity of P450 enzymes, raising the specter that they are heme chaperones (1, 49–53). More recently, they were found to enable the delivery of heme to the nucleus to control metabolism in adipocytes (54). However, current paradigms for heme trafficking and mobilization are heavily protein-centric and often ignore contributions from nucleic acids, which are highly abundant in cells.

The results here provide strong evidence that tentacles of human ribosomes form G4s *in vivo* and that these G4s are involved in appropriating heme. Immunofluorescence experiments with BG4 and L19 antibodies suggest that a specialized fraction of cytosolic ribosomes (~5%) form G4s and that most extra-nuclear G4s (~83%) are ribosomal. The small fraction of ribosomes observed to form G4s *in vivo* contrasts with the high

stability of ribosomal G4s *in vitro* (5, 8). This difference supports Guo and Bartel (20), who suggest that eukaryotic cells have machinery that tends to unfold G4s. Our data show that only a small fraction of potential G4s form *in vivo* and that the fraction can be increased by G4-stabilizing ligands (Fig. 2). The high concentration of rRNA acts in opposition to the low frequency per ribosome so the RNA G4s are abundant. Moreover, the RNA G-quadruplexome appears to be ribosome-centric.

We previously reported that surfaces of both the SSU and the LSU contain G4 sequences (5, 8). A broad variety of data are consistent with more extensive formation of G4s on the LSU than on the SSU. These data include

- more abundant and more expansive G-tracts on the LSU than the SSU (8),
- greater conservation over phylogeny of LSU G-tracts than SSU G-tracts (5, 8),
- higher thermodynamic stability of LSU G4s than SSU G4s (5, 8),
- greater heme-binding to G4 oligomers from the LSU than those from the SSU (Fig. 3A and Fig. S1B),
- greater enrichment of LSU than SSU particles in BioTASQ pulldowns (Fig. 2G),
- greater enrichment of LSU than SSU particles in hemin-agarose pulldowns (Fig. 4A), and
- greater effect of *in vivo* PhenDC3 treatment on LSU than on SSU rRNA in hemin-agarose pulldowns (Fig. 4B).

Our finding that rRNA G4s associate with heme *in vivo* has major implications for the physiology of G4-heme interactions. Decades of *in vitro* biophysical and chemical characterizations indicate that G4 and heme interact with high affinity ( $K_D \sim \text{nM}$ ) and are potent redox catalysts, facilitating peroxidase and peroxxygenase reactions (10–12). However, it remained unclear if heme-G4 complexes form *in vivo* and if heme-G4 catalyzed reactions were physiologically relevant.

The results of three orthogonal approaches from three groups appear to be self-consistent. Maizels and co-workers (35) recently proposed that heme binds to G4s *in vivo*, based on the transcriptional response of cells to PhenDC3. PhenDC3 causes up-regulation of heme-degrading enzymes such as heme oxygenase and other iron and heme homeostatic factors. These responses were interpreted to support a model in which G4s sequester and detoxify heme in cells. Work by Sen and co-workers (13), concurrent with ours, established G4-heme interactions *in vivo* by exploiting the peroxidase activity of G4-heme complexes to self-biotinylate G4s in RNA and DNA using a phenolic-biotin derivative. Here, we demonstrate *in vivo* heme-rRNA<sup>G4</sup> interactions by several methods. The  $K_D$  values for heme-rRNA<sup>G4</sup> complexes (~nM) are on the order of concentration of labile heme (25–300 nM) (40, 55, 56). Therefore, rRNA appears to be poised to buffer labile heme. We propose that heme-rRNA<sup>G4</sup> interactions may be important for protein hemylation reactions and/or for buffering cytosolic heme, mitigating its potential toxicity. It remains to be determined how endogenous factors and processes may modulate G4 formation to regulate heme availability and homeostatic mechanisms.

## Summary

The results here, building on previous *in vitro* work, provide the first demonstration of *in vivo* formation of G4s by rRNA. The levels of rRNA G4 formation observed *in vivo* support a model in which most G-tracts are unfolded in eukaryotes (20). Even so, the extreme density of ribosomes *in vivo* and the large number of G-tracts/ribosome implies a large absolute number of rRNA G4s *in vivo*. We provide evidence that rRNA G4s are inducible by small molecules and can bind heme *in vivo*. The ribosome may help regulate heme bioavailability in cells and may be directly involved in protein hemylation. These results provide new insights into the molecules and mechanisms underlying intracellular heme trafficking and bioavailability, which are currently poorly understood (1–4). Our results suggest that ribosomes, G4-containing rRNAs in particular, may regulate heme metabolism, acting to buffer intracellular heme and possibly regulate heme trafficking and cotranslational hemylation. The ribosome as a potential heme buffer is consistent with its role as a general and versatile sink for ions and small molecules, including antibiotics (57), platinum-based drugs (58–60), metabolites (61), and metal cations  $Mg^{2+}$ ,  $Ca^{2+}$ ,  $Mn^{2+}$ ,  $Fe^{2+}$ , and  $K^+$  (62–67).

## Experimental procedures

### Cell culture

HEK293 cells were cultured in DMEM containing 4.5 g/liter glucose without sodium pyruvate and L-glutamine (Corning) supplemented with 10% FBS (Corning) and 2% penicillin-streptomycin solution (Gibco) in a humidified incubator kept at 37 °C with a 5% carbon dioxide atmosphere.

### RNAs

GQES7-a and GQES7-b were synthesized *in vitro* by transcription (HiScribe™ T7 High Yield RNA Synthesis Kit, New England Biolabs). GQes3 and *mutess3* were purchased from Integrated DNA Technologies. Human 28S and 18S rRNAs were extracted from HEK293 cells with TRIzol (Invitrogen). Intact rRNAs were isolated by pipetting from a native agarose gel after running the rRNA into wells in the center of the gel. The rRNA was then precipitated with 5 M ammonium acetate-acetic acid (pH 7.5) with excess ethanol. RNA sequences are listed in Table S1.

### RNA annealing

RNAs were annealed by heating at 95 °C for 5 min and cooled to 25 °C at 1 °C/min and incubated for 10 min at 4 °C.

### UV-visible absorbance heme-RNA binding

Stock solutions of heme chloride (1 mM) were prepared in DMSO. Prior to use, the heme chloride solution was sonicated for 10 min. RNAs (GQES7-a, GQES7-b, GQes3, and *mutess3*) were annealed as described above in 50 mM KCl and 10 mM Tris-HCl, pH 7.5 in increasing RNA concentrations (for rRNA oligomers: from 0.3 to 1 equivalent of heme). The annealing buffer for intact 28S and 18S rRNAs and assembled ribosomal subunits and polysomes was the same as that of the rRNA

oligomers except for the inclusion of 10 mM  $MgCl_2$ . After RNA annealing, heme was added to a final concentration of 3  $\mu M$ . Samples (20  $\mu l$ ) were allowed to stand at room temperature for 30 min, then loaded onto a Corning 384-well flat clear bottom microplate. Absorbances were recorded from 300 to 700 nm on a BioTek Synergy™ H4 Hybrid plate reader.

### UV-visible absorbance, heme-PhenDC3 competition/cooperation assay

For heme-PhenDC3 competition assays, RNAs were annealed and allowed to bind to heme as above. Final heme concentration was 3  $\mu M$ . Final RNA concentrations were GQES7-a (3  $\mu M$ ), intact human 18S rRNA (65 nM), and intact human 28S rRNA (22 nM). After solutions were incubated for 30 min at room temperature, PhenDC3 or carrier DMSO was added to final concentrations consisting of 1.5  $\mu M$ , 3  $\mu M$ , and 6  $\mu M$ . Samples (20  $\mu l$ ) were allowed to stand at room temperature for 15 min and were loaded onto a Corning 384-well flat clear bottom microplate. Absorbance was recorded from 300 to 700 nm. For PhenDC3-heme cooperation assay (data on Fig. 3G), GQES7-a RNA (1  $\mu M$ ) was added to 3  $\mu M$  heme in 10 mM LiCl and 10 mM Tris-HCl, pH 7.5 with no RNA-annealing step. After RNA-heme solutions were incubated for 30 min at room temperature, PhenDC3 was added to a final concentration range consisting of 1.33–133 nM and allowed to mix for 15 min. The remainder of the experiment was performed as the competition assay described above in this section.

Heme-rRNA dissociation constants were determined from the one-site binding model (68) depicted in the below equations using nonlinear least squares regression analysis software KaleidaGraph 4.5 (Synergy Software, Reading, PA).

$$[rRNA - Hm] = .5 \times (K_D + rRNA_T + Hm_T) - \left( (-K_D - rRNA_T - Hm_T)^2 - 4rRNA_T Hm_T \right)^{.5}$$

$$Abs = Abs_0 + \Delta Abs \times [rRNA - Hm] / [rRNA]_T$$

Where  $K_D$  is the rRNA-heme dissociation constant,  $Hm_T$  is the concentration of heme,  $rRNA-Hm$  is the concentration of the rRNA-heme complex,  $rRNA_T$  is the concentration of rRNA that is being titrated,  $Abs$  is the absorbance at any given concentration of  $rRNA_T$ ,  $Abs_0$  is the initial absorbance of heme in the absence of rRNA, and  $\Delta Abs$  is the change in fluorescence due to the formation of the rRNA-heme complex.

For data fitting,  $Abs_0$ ,  $\Delta Abs$ ,  $rRNA_T$ , and  $Hm_T$  were treated as fixed parameters derived from experiments, and the  $K_D$  was a “floating” parameter that was derived from regression analysis. The absorbance signals utilized to determine  $K_D$  were from the heme Soret band at 400 nm.

### Total heme quantification of untreated and SA-treated HEK293 cells

Heme was quantified as described (69). Briefly, HEK293 cells were seeded in complete DMEM media at an initial confluency of 10% and incubated at 37 °C for 48 h. Media for SA-treated cells was replaced by DMEM supplemented with 10% heme-depleted FBS and 0.5 mM SA. Heme depletion of serum was

## Human ribosomes appropriate heme

performed as described (30). Media for untreated cells was replaced by complete media (supplemented with 10% regular FBS) and allowed to seed at 37 °C for 24 h. The cells were harvested by scrapping and counted using an automated TC10 cell counter (Bio-Rad). Then,  $2.5 \times 10^4$  cells/condition were treated with 20 mM oxalic acid and incubated at 4 °C overnight in the dark. An equal volume of 2 M oxalic acid was added to the cell suspensions. The samples were split, with half incubated at 95 °C for 30 min and half incubated at room temperature for 30 min. The samples were centrifuged at  $21,000 \times g$  for 2 min, 200  $\mu$ l of each was transferred to a black Greiner Bio-One flat bottom fluorescence plate, and porphyrin fluorescence (excitation (ex): 400 nm, emission (em): 620 nm) was recorded on a Synergy Mx multi-modal plate reader. Heme concentration was calculated from a standard curve prepared by diluting a 0.1  $\mu$ M hemin chloride stock solution in DMSO and treated in the same way as the cell suspensions above. To calculate heme concentration, the fluorescence of the unboiled samples was taken as the background level of protoporphyrin IX and subtracted from the fluorescence of the boiled sample, which is used as the free base porphyrin produced upon the release of the heme iron. Using this method, our data suggest SA-treatment of HEK293 cells results in a 7-fold decrease in the total cellular heme concentration.

### Hemin-agarose binding

HEK293 cells were seeded onto a 6-well plate at an initial confluency of 20% in DMEM with 10% FBS and allowed to seed for 48 h at 37 °C. Media was then replaced for DMEM with 10% heme-depleted FBS supplemented with 0.5 mM succinyl acetone (for SA-treated cells). For untreated cells, media was changed for DMEM in 10% regular FBS. Both treated and untreated samples were allowed to incubate at 37 °C for 24 h. The cells were then collected by scrapping and lysed using 1.5-mm zirconium beads (Benchmark Scientific). Lysates were quantified by Bradford assay. In the meantime, hemin-agarose beads and Sepharose beads were equilibrated three times by centrifugation with lysis buffer (0.1% Triton X-100, 10 mM sodium phosphate, 50 mM KCl, 5 mM EDTA, pH 7.5,  $1 \times$  protease arrest, and RNasin RNase Inhibitor (Promega)). 100  $\mu$ l of beads (50- $\mu$ l bed volume) were used per biological replicate. After bead equilibration, each lysate was divided into two and 10  $\mu$ g were loaded to hemin-agarose and 10  $\mu$ g to Sepharose beads. The mixtures were allowed to bind for 60 min, rotating at 20 rpm at room temperature. Then, three washes were performed using lysis buffer and supernatants were discarded. Each wash consisted of 10 min of incubation at room temperature with 20 rpm rotation followed by centrifugation at  $700 \times g$  for 5 min. Bead-bound fractions were eluted by a 15-min incubation at room temperature with 20-rpm rotation in 50  $\mu$ l of 1 M imidazole in lysis buffer, then centrifuged at maximum speed for 2 min, and supernatants were collected. RNA was then extracted from eluted fractions with TRIzol using the manufacturer's protocol. For the PhenDC3 titration in the HEK293 cells experiment, the same protocol was followed, with the difference that the cells were allowed to seed for 24 h (20% initial confluency), and then PhenDC3 was added in increasing con-

centrations (5  $\mu$ M, 10  $\mu$ M, and 20  $\mu$ M). DMSO carrier treatment was performed the same way but with equivalent DMSO volumes. The cells were left at 37 °C for 48 h and collected and lysed as described above.

### RT-qPCR

The sets of primers used can be found in Table S2. Luna Universal One-Step RT-qPCR kit (New England Biolabs) was used following the manufacturer's protocol. Fold enrichments were calculated by comparing the  $C(t)$  values obtained from RNAs extracted from hemin-agarose to RNAs extracted from Sepharose beads. Three biological replicates were performed for all the RT-qPCR experiments. For BioTASQ experiments, fold enrichments were calculated by comparing the  $C(t)$  values obtained from the lysates containing BioTASQ + beads with those containing beads only.

### Heme bioavailability assay using the HS1 sensor

HEK293 cells were plated and transfected in polystyrene-coated sterile 6-well plates (Greiner) for flow cytometry. The cells were plated in basal growth medium DMEM containing 10% FBS. At 30% confluency, the cells were transfected with the heme sensor plasmid pEF52 $\alpha$ -hHS1 using Lipofectamine LTX according to the manufacturer's protocols. After 48 h of treatment with transfection reagents, the cells were treated with PhenDC3 (1 mM stock) in fresh DMEM 10% FBS for 24 h prior to harvesting. Heme-depleted cells were treated with 500  $\mu$ M SA in DMEM containing 10% heme-depleted FBS for 72 h prior to harvesting. Heme-sufficient cells were treated with 350  $\mu$ M ALA in DMEM 10% FBS for 24 h. The cells were harvested in  $1 \times$  PBS for flow analysis. Flow cytometric measurements were performed using a BD FACS Aria III Cell Sorter equipped with an argon laser (ex 488 nm) and a yellow-green laser (ex 561 nm). Enhanced GFP (eGFP) was excited using the argon laser and was measured using a 530/30-nm bandpass filter, and mKate2 was excited using the yellow-green laser and was measured using a 610/20-nm bandpass filter. Data evaluation was conducted using FlowJo v10.4.2 software. Single cells used in the analysis were selected for by first gating for forward scatter and side scatter, consistent with intact cells, and then fluorescence intensities above background were selected by gating for cells with mKate2. The fraction of sensor bound to heme may be quantified according to the following equation (40):

$$\% \text{ Bound} = 100 \times ((R - R_{\min}) / (R_{\max} - R_{\min}))$$

where  $R$  is the median eGFP/mKate2 fluorescence ratio in regular media and  $R_{\min}$  and  $R_{\max}$  are the median sensor ratios when the sensor is depleted of heme or saturated with heme.  $R_{\min}$  and  $R_{\max}$  values are derived from cells cultured in HD+SA or in media conditioned with ALA (40). The plot in Fig. 4D was obtained by fitting the median sensor ratios in Fig. 4C to the following one-site binding model (40, 68):

$$\text{Ratio} = \text{initial ratio} + \Delta\text{ratio} \times (x / (K_d + x))$$

where  $x$  is the independent variable, PhenDC3.

### BG4 purification

pSANG10-3F-BG4 was a gift from Shankar Balasubramanian (Addgene plasmid 55756; RRID:Addgene\_55756). BL21 cells transformed with this plasmid were grown in room temperature and induced overnight with 0.1 mM isopropyl 1-thio- $\beta$ -D-galactopyranoside. The cells were pelleted, then resuspended in xTractor (Takara Bio) supplemented with Protease Arrest (G-Biosciences), lysozyme, and DNase I. Sonicated cell lysate was combined with nickel-nitrilotriacetic acid resin (Invitrogen) and purified via the His-tag. BG4 was further purified by FPLC using a Superdex75 size exclusion column (GE Healthcare).

### Immunofluorescence

Immunofluorescence was performed by standard protocols. HEK293 cells were seeded onto poly-L-lysine-coated cover glass 2 days before the experiment and fixed in 4% formaldehyde for 15 min. The cells were permeabilized with 0.1% Triton X-100 for 3 min and blocked with 5% donkey serum (Jackson ImmunoResearch Laboratories), followed by incubation with antibodies for 1 h at room temperature or overnight at 4°C. Antibodies used here are BG4, rabbit anti-FLAG (Cell Signaling Technology, 14793S), mouse anti-L19 (Santa Cruz Biotechnology, sc-100830), mouse anti-rRNA (Santa Cruz Biotechnology, sc-33678), mouse anti-Calnexin (Santa Cruz Biotechnology, sc-23954), Alexa Fluor 488 conjugated donkey anti-rabbit (Jackson ImmunoResearch Laboratories, 711-545-152), and Rhodamine Red-X conjugated donkey anti-mouse (Jackson ImmunoResearch Laboratories, 715-295150). After staining, the cells were carefully washed with Dulbecco's PBS supplemented with 0.1% Tween 20. Nuclear DNA was stained with 4',6-diamidino-2-phenylindole. Images were acquired with a Zeiss 700 Laser Scanning Confocal Microscope. PhenDC3 treatment consisted of incubation at 37°C overnight at 10  $\mu$ M. PhenDC3 treatment was done prior to cell fixation. Determination of colocalization ratios was performed as described in Zen software (Zeiss). No-primary-antibody controls and RNase A- and PhenDC3-treated images are reported in Fig. S6 and Fig. S7. The *colocalization* image in Fig. 2, A and B shows the G4 signal that colocalizes with L19 and with the ER (*yellow pixels*) and the one that does not colocalize (*green pixels*). L19, ER, and BG4 images only present their respective fluorescence signals.

### BioTASQ capture of cellular RNAs

BioTASQ experiments followed published protocols *in vitro* (8) and *in vivo* (22). Briefly, HEK293 cells were seeded onto a 6-well plate at 20% confluency and allowed to incubate at 37°C for 48 h. The cells were then cross-linked with 1% paraformaldehyde/PBS for 5 min at room temperature. Cross-linking was stopped by incubating cells with 0.125 M glycine for 5 min at room temperature. The cells were harvested by scrapping and resuspended in lysis buffer (200 mM KCl, 25 mM Tris-HCl, pH 7.5, 5 mM EDTA, 0.5 mM DTT, 1% Triton X-100, RNasin RNase Inhibitor, and 1 $\times$  protease arrest). The cells were lysed by sonication (30% amplitude, 10 s on and off intervals, and 2 min sonication time). The lysate was then split: BioTASQ was added at a final concentration of 100  $\mu$ M to one of the samples, and the other sample was left untreated. The lysates were incubated at

4°C overnight with gentle rotation. Sera-Mag magnetic streptavidin-coated beads (GE Healthcare) were washed three times with wash buffer (5 mM Tris-HCl, pH 7.5, 0.5 mM EDTA, and 1 M KCl). Each wash was followed by centrifugation at 3,500 rpm for 5 min at 4°C. The beads were then treated with buffer 1 (0.1 M NaOH, and 0.05 M KCl in RNase/DNase-free water) two times at room temperature for 2 min and then centrifuged at 3,500 rpm at 4°C for 5 min and washed with buffer 2 (0.1 M KCl in RNase/DNase-free water). Lastly, to block, the beads were treated with 1  $\mu$ g/ml BSA and 1  $\mu$ g/ml yeast tRNA and allowed to incubate at 4°C overnight with gentle rotation.

After incubation overnight with BioTASQ, the cell lysates were treated with 1% BSA for 1 h at 4°C. Washed magnetic beads were added to the lysates (20  $\mu$ g beads/sample) and allowed to mix with gentle rotation at 4°C for 1 h. The beads were then washed three times with lysis buffer for 5 min, and then cross-linking was reversed by incubating the beads at 70°C for 1 h. Finally, TRIzol was used to extract RNAs for analysis by RT-qPCR.

### Data availability

All data are contained within this article and in the [supporting information](#).

**Acknowledgments**—We thank Drs. Rebecca Donegan, David A. Hanna, Jonathan B. Chaires, Aaron Engelhart, David Monchaud, and Judy Wong, and Claudia Montllor-Albalade for helpful discussions. We acknowledge Andrew Shaw and the core facilities at the Parker H. Petit Institute for Bioengineering and Bioscience at the Georgia Institute of Technology for expert advice and the use of equipment. Purified human ribosomes and polysomes were a gift from Immagina BioTechnology. BioTASQ was a gift from Dr. David Monchaud.

**Author contributions**—S. M.-F., A. R. R., and L. D. W. conceptualization; S. M.-F., C. I., C. M. M., and A. R. R. data curation; S. M.-F., and C. I. formal analysis; S. M.-F. and C. I. validation; S. M.-F., C. I., and C. M. M. investigation; S. M.-F. and C. I. visualization; S. M.-F. methodology; S. M.-F., A. R. R., and L. D. W. writing-original draft; A. R. R. and L. D. W. resources; A. R. R. and L. D. W. supervision; A. R. R. and L. D. W. funding acquisition; A. R. R. and L. D. W. project administration.

**Funding and additional information**—This work was supported by NASA Grants 80NSSC17K0295 and 80NSSC18K1139 (Center for the Origin of Life) (to L. D. W.), the National Institutes of Health Grant ES025661 (to A. R. R.), and the National Science Foundation Grant MCB-1552791 (to A. R. R.). The content is solely the responsibility of the authors and does not necessarily represent the official views of the National Institutes of Health.

**Conflict of interest**—The authors declare that they have no conflict of interest with the contents of this article.

**Abbreviations**—The abbreviations used are: G4, G-quadruplex; rProtein, ribosomal protein; ER, endoplasmic reticulum; SSU, small

subunit; LSU, large subunit; SA, succinylacetone; HS, heme sensor; HD+SA, heme-deficient media containing SA; ALA, 5-aminolevulinic acid; eGFP, enhanced GFP; ex, excitation; em, emission.

## References

- Swenson, S. A., Moore, C. M., Marcero, J. R., Medlock, A. E., Reddi, A. R., and Khalimonchuk, O. (2020) From synthesis to utilization: the ins and outs of mitochondrial heme. *Cells* **9**, 579 [CrossRef Medline](#)
- Donegan, R. K., Moore, C. M., Hanna, D. A., and Reddi, A. R. (2019) Handling heme: the mechanisms underlying the movement of heme within and between cells. *Free Radic. Biol. Med.* **133**, 88–100 [CrossRef Medline](#)
- Hanna, D. A., Martinez-Guzman, O., and Reddi, A. R. (2017) Heme gazing: illuminating eukaryotic heme trafficking, dynamics, and signaling with fluorescent heme sensors. *Biochemistry* **56**, 1815–1823 [CrossRef Medline](#)
- Reddi, A. R., and Hamza, I. (2016) Heme mobilization in animals: a metal-lipid's journey. *Acc. Chem. Res.* **49**, 1104–1110 [CrossRef Medline](#)
- Mestre-Fos, S., Penev, P. I., Suttapitugsakul, S., Hu, M., Ito, C., Petrov, A. S., Wartell, R. M., Wu, R., and Williams, L. D. (2019) G-quadruplexes in human ribosomal RNA. *J. Mol. Biol.* **431**, 1940–1955 [CrossRef Medline](#)
- Bowman, J. C., Petrov, A. S., Frenkel-Pinter, M., Penev, P. I., and Williams, L. D. (2020) Root of the tree: the significance, evolution, and origins of the ribosome. *Chem. Rev.* **120**, 4848–4878 [CrossRef](#)
- Melnikov, S., Ben-Shem, A., De Loubresse, N. G., Jenner, L., Yusupova, G., and Yusupov, M. (2012) One core, two shells: bacterial and eukaryotic ribosomes. *Nat. Struct. Mol. Biol.* **19**, 560–567 [CrossRef Medline](#)
- Mestre-Fos, S., Penev, P. I., Richards, J. C., Dean, W. L., Gray, R. D., Chaires, J. B., and Williams, L. D. (2019) Profusion of G-quadruplexes on both subunits of metazoan ribosomes. *PLoS ONE* **14**, e0226177 [CrossRef Medline](#)
- Milo, R., and Phillips, R. (2015) *Cell biology by the numbers*. Garland Science [CrossRef](#)
- Poon, L. C.-H., Methot, S. P., Morabi-Pazooki, W., Pio, F., Bennet, A. J., and Sen, D. (2011) Guanine-rich RNAs and DNAs that bind heme robustly catalyze oxygen transfer reactions. *J. Am. Chem. Soc.* **133**, 1877–1884 [CrossRef Medline](#)
- Sen, D., and Poon, L. C. (2011) RNA and DNA complexes with hemin [Fe (III) heme] are efficient peroxidases and peroxygenases: how do they do it and what does it mean? *Crit. Rev. Biochem. Mol. Biol.* **46**, 478–492 [CrossRef Medline](#)
- Li, Y., and Sen, D. (1996) A catalytic DNA for porphyrin metallation. *Nat. Struct. Biol.* **3**, 743–747 [CrossRef Medline](#)
- Lat, P. K., Liu, K., Kumar, D. N., Wong, K. K. L., Verheyen, E. M., and Sen, D. (2020) High specificity and tight spatial restriction of self-biotinylation by DNA and RNA G-quadruplexes complexed *in vitro* and *in vivo* with heme. *Nucleic Acids Res.* **48**, 5254–5267 [CrossRef Medline](#)
- Paeschke, K., Capra, J. A., and Zakian, V. A. (2011) DNA replication through G-quadruplex motifs is promoted by the *saccharomyces cerevisiae* Pif1 DNA helicase. *Cell* **145**, 678–691 [CrossRef Medline](#)
- Siddiqui-Jain, A., Grand, C. L., Bearss, D. J., and Hurley, L. H. (2002) Direct evidence for a G-quadruplex in a promoter region and its targeting with a small molecule to repress *c-MYC* transcription. *Proc. Natl. Acad. Sci. U.S.A.* **99**, 11593–11598 [CrossRef Medline](#)
- Ribeyre, C., Lopes, J., Boulé, J.-B., Piazza, A., Guédin, A., Zakian, V. A., Mergny, J.-L., and Nicolas, A. (2009) The yeast Pif1 helicase prevents genomic instability caused by G-quadruplex-forming CEB1 sequences *in vivo*. *PLoS Genet.* **5**, e1000475 [CrossRef Medline](#)
- Beaudoin, J.-D., and Perreault, J.-P. (2010) 5'-UTR G-quadruplex structures acting as translational repressors. *Nucleic Acids Res.* **38**, 7022–7036 [CrossRef Medline](#)
- Arora, A., Dutkiewicz, M., Scaria, V., Hariharan, M., Maiti, S., and Kurreck, J. (2008) Inhibition of translation in living eukaryotic cells by an RNA G-quadruplex motif. *RNA* **14**, 1290–1296 [CrossRef Medline](#)
- Kumari, S., Bugaut, A., Huppert, J. L., and Balasubramanian, S. (2007) An RNA G-quadruplex in the 5' UTR of the *NRAS* proto-oncogene modulates translation. *Nat. Chem. Biol.* **3**, 218–221 [CrossRef Medline](#)
- Guo, J. U., and Bartel, D. P. (2016) RNA G-quadruplexes are globally unfolded in eukaryotic cells and depleted in bacteria. *Science* **353**, aaf5371 [CrossRef Medline](#)
- Fay, M. M., Lyons, S. M., and Ivanov, P. (2017) RNA G-quadruplexes in biology: principles and molecular mechanisms. *J. Mol. Biol.* **429**, 2127–2147 [CrossRef Medline](#)
- Yang, S. Y., Lejault, P., Chevrier, S., Boidot, R., Robertson, A. G., Wong, J. M., and Monchaud, D. (2018) Transcriptome-wide identification of transient RNA G-quadruplexes in human cells. *Nat. Commun.* **9**, 4730 [CrossRef Medline](#)
- Biffi, G., Di Antonio, M., Tannahill, D., and Balasubramanian, S. (2014) Visualization and selective chemical targeting of RNA G-quadruplex structures in the cytoplasm of human cells. *Nat. Chem.* **6**, 75–80 [CrossRef Medline](#)
- Biffi, G., Tannahill, D., McCafferty, J., and Balasubramanian, S. (2013) Quantitative visualization of DNA G-quadruplex structures in human cells. *Nat. Chem.* **5**, 182–186 [CrossRef Medline](#)
- Moye, A. L., Porter, K. C., Cohen, S. B., Phan, T., Zyner, K. G., Sasaki, N., Lovrecz, G. O., Beck, J. L., and Bryan, T. M. (2015) Telomeric G-quadruplexes are a substrate and site of localization for human telomerase. *Nat. Commun.* **6**, 7643 [CrossRef Medline](#)
- Conlon, E. G., Lu, L., Sharma, A., Yamazaki, T., Tang, T., Shneider, N. A., and Manley, J. L. (2016) The C9ORF72 GGGGCC expansion forms RNA G-quadruplex inclusions and sequesters hnRNP H to disrupt splicing in ALS brains. *eLife* **5**, e17820 [CrossRef Medline](#)
- Hänsel-Hertsch, R., Beraldi, D., Lensing, S. V., Marsico, G., Zyner, K., Parry, A., Di Antonio, M., Pike, J., Kimura, H., Narita, M., Tannahill, D., and Balasubramanian, S. (2016) G-quadruplex structures mark human regulatory chromatin. *Nat. Genet.* **48**, 1267–1272 [CrossRef Medline](#)
- Laguerre, A., Wong, J. M., and Monchaud, D. (2016) Direct visualization of both DNA and RNA quadruplexes in human cells via an uncommon spectroscopic method. *Sci. Rep.* **6**, 32141 [CrossRef Medline](#)
- Monchaud, D., Allain, C., Bertrand, H., Smargiasso, N., Rosu, F., Gabelica, V., De Cian, A., Mergny, J.-L., and Teulade-Fichou, M.-P. (2008) Ligands playing musical chairs with G-quadruplex DNA: a rapid and simple displacement assay for identifying selective G-quadruplex binders. *Biochimie* **90**, 1207–1223 [CrossRef Medline](#)
- De Cian, A., Delemos, E., Mergny, J.-L., Teulade-Fichou, M.-P., and Monchaud, D. (2007) Highly efficient G-quadruplex recognition by bisquinolinium compounds. *J. Am. Chem. Soc.* **129**, 1856–1857 [CrossRef Medline](#)
- Piazza, A., Boulé, J.-B., Lopes, J., Mingo, K., Largy, E., Teulade-Fichou, M.-P., and Nicolas, A. (2010) Genetic instability triggered by G-quadruplex interacting Phen-DC compounds in *Saccharomyces cerevisiae*. *Nucleic Acids Res.* **38**, 4337–4348 [CrossRef Medline](#)
- Bonnat, L., Bar, L., Génaro, B., Bonnet, H., Jarjayes, O., Thomas, F., Dejeu, J., Defrancq, E., and Lavergne, T. (2017) Template-mediated stabilization of a DNA G-quadruplex formed in the HIV-1 promoter and comparative binding studies. *Chem. Eur. J.* **23**, 5602–5613 [CrossRef Medline](#)
- Reid, D. W., and Nicchitta, C. V. (2012) Primary role for endoplasmic reticulum-bound ribosomes in cellular translation identified by ribosome profiling. *J. Biol. Chem.* **287**, 5518–5527 [CrossRef Medline](#)
- Renard, I., Grandmougin, M., Roux, A., Yang, S. Y., Lejault, P., Pirrotta, M., Wong, J. M., and Monchaud, D. (2019) Small-molecule affinity capture of DNA/RNA quadruplexes and their identification *in vitro* and *in vivo* through the G4RP protocol. *Nucleic Acids Res.* **47**, 5502–5510 [CrossRef Medline](#)
- Gray, L. T., Lombardi, E. P., Verga, D., Nicolas, A., Teulade-Fichou, M.-P., Londoño-Vallejo, A., and Maizels, N. (2019) G-quadruplexes sequester free heme in living cells. *Cell Chem. Biol.* **26**, 1681–1691.e5 [CrossRef Medline](#)
- Shimizu, H., Tai, H., Saito, K., Shibata, T., Kinoshita, M., and Yamamoto, Y. (2015) Characterization of the interaction between heme and a parallel G-quadruplex DNA formed from d(TTAGGGT). *Bull. Chem. Soc. Jpn.* **88**, 644–652 [CrossRef](#)
- Saito, K., Tai, H., Hemmi, H., Kobayashi, N., and Yamamoto, Y. (2012) Interaction between the heme and a G-quartet in a heme-DNA complex. *Inorg. Chem.* **51**, 8168–8176 [CrossRef Medline](#)

38. Shinomiya, R., Katahira, Y., Araki, H., Shibata, T., Momotake, A., Yanagisawa, S., Ogura, T., Suzuki, A., Neya, S., and Yamamoto, Y. (2018) Characterization of catalytic activities and heme coordination structures of heme–DNA complexes composed of some chemically modified hemes and an all parallel-stranded tetrameric G-quadruplex DNA formed from d(TTAGGG). *Biochemistry* **57**, 5930–5937 [CrossRef Medline](#)
39. Grigg, J. C., Shumayrikh, N., and Sen, D. (2014) G-quadruplex structures formed by expanded hexanucleotide repeat RNA and DNA from the neurodegenerative disease-linked C9orf72 gene efficiently sequester and activate heme. *PLoS ONE* **9**, e106449 [CrossRef Medline](#)
40. Hanna, D. A., Harvey, R. M., Martinez-Guzman, O., Yuan, X., Chandrasekharan, B., Raju, G., Outten, F. W., Hamza, I., and Reddi, A. R. (2016) Heme dynamics and trafficking factors revealed by genetically encoded fluorescent heme sensors. *Proc. Natl. Acad. Sci. U.S.A.* **113**, 7539–7544 [CrossRef Medline](#)
41. Ebert, P. S., Hess, R. A., Frykholm, B. C., and Tschudy, D. P. (1979) Succinylacetone, a potent inhibitor of heme biosynthesis: effect on cell growth, heme content and  $\delta$ -aminolevulinic acid dehydratase activity of malignant murine erythroleukemia cells. *Biochem. Biophys. Res. Commun.* **88**, 1382–1390 [CrossRef Medline](#)
42. Hanna, D. A., Hu, R., Kim, H., Martinez-Guzman, O., Torres, M. P., and Reddi, A. R. (2018) Heme bioavailability and signaling in response to stress in yeast cells. *J. Biol. Chem.* **293**, 12378–12393 [CrossRef Medline](#)
43. Sweeny, E. A., Singh, A. B., Chakravarti, R., Martinez-Guzman, O., Saini, A., Haque, M. M., Garee, G., Dans, P. D., Hannibal, L., Reddi, A. R., and Stuehr, D. J. (2018) Glyceraldehyde-3-phosphate dehydrogenase is a chaperone that allocates labile heme in cells. *J. Biol. Chem.* **293**, 14557–14568 [CrossRef Medline](#)
44. Martinez-Guzman, O., Willoughby, M. M., Saini, A., Dietz, J. V., Bohoych, I., Medlock, A. E., Khalimonchuk, O., and Reddi, A. R. (2020) Mitochondrial–nuclear heme trafficking in budding yeast is regulated by GTPases that control mitochondrial dynamics and ER contact sites. *J. Cell Sci.* **133**, jcs237917 [CrossRef](#)
45. Hannibal, L., Collins, D., Brassard, J., Chakravarti, R., Vempati, R., Dorlet, P., Santolini, J. R. M., Dawson, J. H., and Stuehr, D. J. (2012) Heme binding properties of glyceraldehyde-3-phosphate dehydrogenase. *Biochemistry* **51**, 8514–8529 [CrossRef Medline](#)
46. Chakravarti, R., Aulak, K. S., Fox, P. L., and Stuehr, D. J. (2010) GAPDH regulates cellular heme insertion into inducible nitric oxide synthase. *Proc. Natl. Acad. Sci. U.S.A.* **107**, 18004–18009 [CrossRef Medline](#)
47. Dai, Y., Sweeny, E. A., Schlanger, S., Ghosh, A., and Stuehr, D. J. (2020) GAPDH delivers heme to soluble guanylyl cyclase. *J. Biol. Chem.* **295**, 8145–8154 [CrossRef Medline](#)
48. Piel, I. I. R., Shiferaw, M. T., Vashisht, A. A., Marcero, J. R., Praissman, J. L., Phillips, J. D., Wohlschlegel, J. A., and Medlock, A. E. (2016) A novel role for progesterone receptor membrane component 1 (PGRMC1): a partner and regulator of ferrochelatase. *Biochemistry* **55**, 5204–5217 [CrossRef Medline](#)
49. Craven, R. J., Mallory, J. C., and Hand, R. A. (2007) Regulation of iron homeostasis mediated by the heme-binding protein Dap1 (damage resistance protein 1) via the p450 protein Erg11/Cyp51. *J. Biol. Chem.* **282**, 36543–36551 [CrossRef Medline](#)
50. Mallory, J. C., Crudden, G., Johnson, B. L., Mo, C., Pierson, C. A., Bard, M., and Craven, R. J. (2005) Dap1p, a heme-binding protein that regulates the cytochrome p450 protein Erg11p/Cyp51p in *Saccharomyces cerevisiae*. *Mol. Cell Biol.* **25**, 1669–1679 [CrossRef Medline](#)
51. Ghosh, K., Thompson, A. M., Goldbeck, R. A., Shi, X., Whitman, S., Oh, E., Zhiwu, Z., Vulpe, C., and Holman, T. R. (2005) Spectroscopic and biochemical characterization of heme binding to yeast Dap1p and mouse PGRMC1p. *Biochemistry* **44**, 16729–16736 [CrossRef Medline](#)
52. Thompson, A. M., Reddi, A. R., Shi, X., Goldbeck, R. A., Moënn-Loccoz, P., Gibney, B. R., and Holman, T. R. (2007) Measurement of the heme affinity for yeast dap1p, and its importance in cellular function. *Biochemistry* **46**, 14629–14637 [CrossRef Medline](#)
53. Hughes, A. L., Powell, D. W., Bard, M., Eckstein, J., Barbuch, R., Link, A. J., and Espenshade, P. J. (2007) Dap1/PGRMC1 binds and regulates cytochrome p450 enzymes. *Cell Metab.* **5**, 143–149 [CrossRef Medline](#)
54. Galmozzi, A., Kok, B. P., Kim, A. S., Montenegro-Burke, J. R., Lee, J. Y., Spreafico, R., Mosure, S., Albert, V., Cintron-Colon, R., Godio, C., Webb, W. R., Conti, B., Solt, L. A., Kojetin, D., Parker, C. G., et al. (2019) PGRMC2 is an intracellular haem chaperone critical for adipocyte function. *Nature* **576**, 138–142 [CrossRef Medline](#)
55. Yuan, X., Rietzschel, N., Kwon, H., Nuno, A. B. W., Hanna, D. A., Phillips, J. D., Raven, E. L., Reddi, A. R., and Hamza, I. (2016) Regulation of intracellular heme trafficking revealed by subcellular reporters. *Proc. Natl. Acad. Sci. U.S.A.* **113**, E5144–E5152 [CrossRef Medline](#)
56. Song, Y., Yang, M., Wegner, S. V., Zhao, J., Zhu, R., Wu, Y., He, C., and Chen, P. R. (2015) A genetically encoded fret sensor for intracellular heme. *ACS Chem. Biol.* **10**, 1610–1615 [CrossRef Medline](#)
57. Wilson, D. N. (2014) Ribosome-targeting antibiotics and mechanisms of bacterial resistance. *Nat. Rev. Microbiol.* **12**, 35–48 [CrossRef Medline](#)
58. Hostetter, A. A., Osborn, M. F., and Deroose, V. J. (2012) RNA-pt adducts following cisplatin treatment of *Saccharomyces cerevisiae*. *ACS Chem. Biol.* **7**, 218–225 [CrossRef Medline](#)
59. Plakos, K., and Deroose, V. J. (2017) Mapping platinum adducts on yeast ribosomal RNA using high-throughput sequencing. *Chem. Commun.* **53**, 12746–12749 [CrossRef Medline](#)
60. Rijal, K., and Chow, C. S. (2008) A new role for cisplatin: probing ribosomal RNA structure. *Chem. Commun.*
61. Del Valle, A. H., Seip, B., Cervera-Marzal, I., Sacheau, G., Seefeldt, A. C., and Innis, C. A. (2020) Ornithine capture by a translating ribosome controls bacterial polyamine synthesis. *Nat. Microbiol.* 1–8 [Medline](#)
62. Gesteland, R. F. (1966) Unfolding of *Escherichia coli* ribosomes by removal of magnesium. *J. Mol. Biol.* **18**, 356–371 [CrossRef Medline](#)
63. Stahl, C., and Noll, H. (1977) Structural dynamics of bacterial ribosomes. *Mol. Gen. Genet. MGG* **153**, 159–168 [CrossRef Medline](#)
64. Weiss, R. L., Kimes, B. W., and Morris, D. R. (1973) Cations and ribosome structure. III. Effects on the 30S and 50S subunits of replacing bound  $Mg^{2+}$  by inorganic cations. *Biochemistry* **12**, 450–456 [CrossRef Medline](#)
65. Gordon, J., and Lipmann, F. (1967) Role of divalent ions in poly U-directed phenylalanine polymerization. *J. Mol. Biol.* **23**, 23–33 [CrossRef](#)
66. Nierhaus, K. H. (2014)  $Mg^{2+}$ ,  $K^+$ , and the ribosome. *J. Bacteriol.* **196**, 3817–3819 [CrossRef Medline](#)
67. Bray, M. S., Lenz, T. K., Haynes, J. W., Bowman, J. C., Petrov, A. S., Reddi, A. R., Hud, N. V., Williams, L. D., and Glass, J. B. (2018) Multiple prebiotic metals mediate translation. *Proc. Natl. Acad. Sci. U.S.A.* **115**, 12164–12169 [CrossRef Medline](#)
68. Sankar, S. B., Donegan, R. K., Shah, K. J., Reddi, A. R., and Wood, L. B. (2018) Heme and hemoglobin suppress amyloid  $\beta$ -mediated inflammatory activation of mouse astrocytes. *J. Biol. Chem.* **293**, 11358–11373 [CrossRef Medline](#)
69. Sinclair, P. R., Gorman, N., and Jacobs, J. M. (1999) Measurement of heme concentration. *Curr. Protoc. Toxicol.* 8.3.1–8.3.7 [CrossRef](#)
70. Zhu, Y., Hon, T., Ye, W., and Zhang, L. (2002) Heme deficiency interferes with the Ras-mitogen-activated protein kinase signaling pathway and expression of a subset of neuronal genes. *Cell Growth Differ.* **13**, 431–439 [Medline](#)

**Human ribosomal G-quadruplexes regulate heme bioavailability**  
Santi Mestre-Fos, Chieri Ito, Courtney M. Moore, Amit R. Reddi and Loren Dean  
Williams

*J. Biol. Chem.* 2020, 295:14855-14865.

doi: 10.1074/jbc.RA120.014332 originally published online August 13, 2020

---

Access the most updated version of this article at doi: [10.1074/jbc.RA120.014332](https://doi.org/10.1074/jbc.RA120.014332)

Alerts:

- [When this article is cited](#)
- [When a correction for this article is posted](#)

[Click here](#) to choose from all of JBC's e-mail alerts

This article cites 69 references, 17 of which can be accessed free at  
<http://www.jbc.org/content/295/44/14855.full.html#ref-list-1>